Molecular Structure and Precipitates of a Rodlike Polysaccharide in Aqueous Solution by SAXS Experiments

M. Gawronski,*,† G. Aguirre,‡ H. Conrad,† T. Springer,† and K.-P. Stahmann§

Institut für Festkörperforschung and Institut für Biotechnologie, Forschungszentrum Jülich GmbH, D-52425 Jülich, Germany, and Université de Bordeaux I, F-33405 Talence Cedex, France

Received September 12, 1995; Revised Manuscript Received December 7, 1995⊗

ABSTRACT: Cinerean is a microbial β-(1−3)(1−6)-D-glucan produced by the fungus *Botrytis cinerea*. The native cinerean molecule is a wormlike chain with a large persistence length. Fragments are formed by sonication that are nearly rigid rods. The mass per unit length of these rods (M/L = 2400 ± 300 Da nm^{-1}) and their diameter (D = 1.7 ± 0.2 nm) were determined by small-angle X-ray scattering (SAXS). From these results, a triple-helical conformation for the cinerean molecules can be concluded, which accounts for the rigidity of the rods. Fragmented cinerean in aqueous solution shows a phase diagram explained qualitatively by Flory's theory for rigid rods. SAXS experiments in the miscibility gap reveal a diffraction peak at Q_M = 0.37 Å^{-1} for H_2O as solvent. For close packing of the rods this Debye−Scherrer ring leads to a diameter of 1.9 nm, which is consistent with the value from experiments in the isotropic phase.

Introduction

Cinerean is a microbial polysaccharide produced by the fungus *Botrytis cinerea* for extracellular energy storage when grown in medium with glucose as the only carbon source.[1,2] It is a β-(1−3)(1−6)-D-glucan. D-glucans are formed by D-glycopyranose rings that are connected by glucosidic linkages.[3] For some D-glucans it was shown that they affect the immune system as an unspecific modulator that might be of use in a cure for certain kinds of cancer.[4,5] These polysaccharides achieve technical importance[6] in tertiary oil recovery[7] and as gelation agents in the food industry, because even a few grams per liter of the native forms make aqueous solutions highly viscous.

We are interested in cinerean as a model substance for very long, stiff molecules that are used for spinning and the production of fibers.[8] From electron microscopy it is known that the native cinerean molecule is a wormlike chain with a large persistence length.[9] Nearly rigid rodlike fragments can be formed by sonication.[9] In solution rodlike molecules reveal a phase separation with a miscibility gap. Depending on temperature and concentration, the rods were predicted to align in bundle-shaped domains.[10] The phase diagram of sonicated cinerean for low concentrations is shown in our recent paper.[9] The main goal of this work is the investigation of these precipitates of cinerean with small-angle X-ray scattering (SAXS) in the two-phase region of the phase diagram. In addition, the morphology of the fragments in the homogeneous phase is examined with SAXS. From the measured scattering curve, the mass density per length and the diameter of the rods were determined.

Other research groups have thoroughly examined a similar polysaccharide called schizophyllan (produced by the fungus *Schizophyllum commune*). By calorimetric measurements[11] and by measurements of the molecular weight and viscosity,[12] it was shown that schizophyllan has a triple-helical conformation in aqueous solutions. It was observed that the rodlike triple helix disentangles at higher temperatures. When dissolved in NaOH solutions or in dimethyl sulfoxide (DMSO), it decomposes into three single strands with the conformation of a random coil. Obviously the triple-helical conformation accounts for the rigidity of the rod. We describe this helix−coil transition for cinerean, depending on the pH value of the solution examined with SAXS, in another paper.[13] It has been shown that sonicated schizophyllan forms a cholesteric mesophase at high concentrations.[14] With optical rotation and heat capacity measurements, the transition between the isotropic phase and the cholesteric mesophase has been investigated.[15]

To our knowledge, this is the first paper that examines the precipitated phase of polysaccharide solutions with SAXS.

Experimental Section

Cultivation of *Botrytis cinerea* and Cinerean Production. The *Botrytis cinerea* strain LU 478 MaB was cultivated in a mineral salt medium, with D-glucose as the sole carbon source. The exact conditions for the cultivation and precipitation were described by Stahmann et al.[2]

Sonication. The native cinerean was sonicated with a Branson B-15 P instrument. During the sonication the sample was kept at a temperature of about 8 °C. To remove metal fragments from the $^1/_2$ in. horn of the sonifier, the sonicated sample was centrifuged at 42000*g* for 35 min. The fragments were precipitated by adding 2-propanol. After centrifugation at 4000*g*, the resulting pellet was dried in an argon flow until the weight remained unchanged.

Low-angle laser light_scattering yields the weight-average molecular masses M of the samples.[9]

Small-Angle X-ray Scattering (SAXS). The SAXS measurements were partly performed at the JUSIFA, a small-angle scattering facility in Jülich that uses a 100 kW rotating copper anode. Further measurements were carried out on the same instrument at DESY/Hasylab in Hamburg, with the DORIS storage ring as the X-ray source.[16] The scattered intensity is measured with a two-dimensional position-sensitive detector. To obtain the mass per unit length, a standard scatterer of amorphous carbon was used for calibration on an absolute scale. The X-ray energies were 8 keV at the Cu Kα edge and 12 keV at the synchrotron.

* Corresponding author.
† Institut für Festkörperforschung, Forschungszentrum Jülich GmbH.
‡ Université de Bordeaux I.
§ Institut für Biotechnologie, Forschungszentrum Jülich GmbH.
⊗ Abstract published in *Advance ACS Abstracts,* February 1, 1996.

0024-9297/96/2229-1516$12.00/0

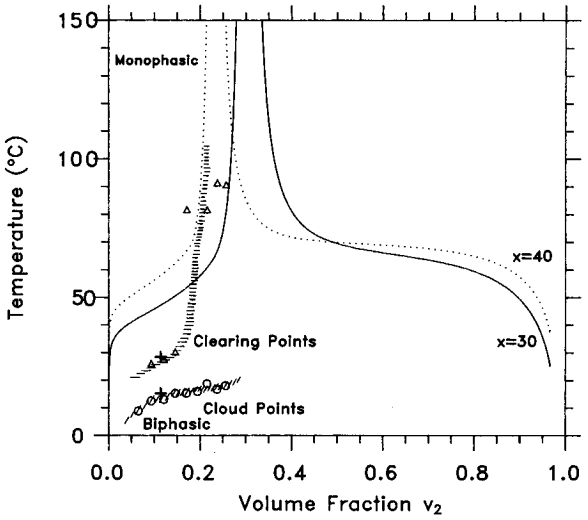

Figure 1. Theoretical phase diagram for axis ratios $x = L/D = 30$ and $x = 40$ in comparison with the measured values. The solutions used for X-ray scattering are marked with +. The shaded region is a guideline for the eye to show the phase boundary.

Results and Discussion

Phase Separation. The length distribution of the fragmented cinerean is relatively narrow, as shown by gel-permeation chromatography and electron microscopy.[9] With cloud point measurements and viscometry, we obtained a partial phase diagram for fragmented cinerean.[9]

Figure 1 shows the results of our previous measurements, including where our SAXS measurements were carried out. According to Flory's theory for rigid rods,[10] at low concentrations and for sufficiently high temperatures the rods are distributed randomly and the solution is isotropic. In certain concentration and temperature ranges, precipitates occur in an otherwise isotropic solution. Experimentally, the solution is turbid. By varying the temperature it is possible to pass from the isotropic to the turbid solution reversibly. The clearing and cloud points show a strong hysteresis.[9]

Conformation of Fragmented Cinerean in an Isotropic Solution. SAXS is a powerful method to investigate the conformation of these particles in their natural aqueous environment. The intensity scattered into a resolution element of the detector is given by

$$\Delta I(Q) = j_0 nFDT[\mathrm{d}\sigma(Q)/\mathrm{d}\Omega]\Delta\Omega$$

with $n = cN_A/M$ and $j_0 = I_0/F$. Here $\mathrm{d}\sigma/\mathrm{d}\Omega$ is the scattering cross section per particle, j_0 is the current density of the primary beam, F is the irradiated area, D is the sample thickness, T is the transmission of the sample, n is the number density of the particles, c is the concentration of the particles in the solution, N_A is Avogadro's number, M is the molecular mass of the particles, and I_0 is the primary intensity. Q is the absolute value of the scattering vector, which is connected to the scattering angle 2θ and the wavelength λ of the incident radiation by $Q = (4\pi/\lambda)\sin(\theta) \approx 4\pi\theta/\lambda$.

The scattering cross section of rodlike particles randomly orientated in a solution is given by[17]

$$\mathrm{d}\sigma/\mathrm{d}\Omega = \sigma_{Th}(\Delta\varrho_e)^2 A_c^{\,2}\pi L(1/Q)\exp[-(R_c^{\,2}Q^2)/2] \qquad (1)$$

for $2\pi/L \ll Q \ll 2\pi/R$. Here σ_{Th} is the differential Thomson cross section of the electron, $\Delta\rho_e$ is the averaged electron density difference between the particles and the solvent, A_c the area of the cross section of the rod, and L is its length. R_c is the mean square radius of the electron density in a plane perpendicular to the rod axis.[17] By assuming for simplicity that the particles can be described as a cylinder with a sharp surface being filled homogeneously with electrons, an effective radius R of the rod can be calculated. It is related to the mean square radius of the electron density by[17] $R = \sqrt{2}R_c$.

Together with $\Delta\rho_e = (M\Delta z)/(LA_c)$ and $n = (cN_A)/M$, these formulae yield the macroscopic scattering cross section from a SAXS experiment:

$$\mathrm{d}\Sigma/\mathrm{d}\Omega = n(\mathrm{d}\sigma/\mathrm{d}\Omega) = \frac{\Delta I/\Delta\Omega}{I_0 DT} = \sigma_{Th}\pi N_A(\Delta z)^2 c(M/L)(1/Q)\exp[-(Q^2R^2)/4] \qquad (2)$$

M is the molecular mass of the particles, Δz is the difference in mole electrons per gram between the particle and the solvent, c is the concentration of the particles in the solution, and n is the number density of the particles. Only the mass per length M/L enters, which is obtained with eq 2 from the Q^{-1} region. It is necessary to know the macroscopic density of the substance and to measure the macroscopic scattering cross section on an absolute scale. The result for M/L is the same for polydisperse systems with a length distribution, because the rods only differ in their length and not their mass per length.

Typical scattering curves for isotropic solutions of fragmented cinerean in H_2O and D_2O are shown in Figure 2a,b. The Guinier regime containing information on the radius of gyration R_G and the molecular mass M of the *whole* particle could not be reached due to its length ($R_G \gg 1/Q$). The rise of the curve for very low Q values in D_2O is caused by agglomerates. For water the Q^{-1} regime expected for $Q \ll 2\pi/R$ is well developed over almost one decade in Q. It only contains information on M/L. For high Q values, a Q^{-4} behavior is expected according to Porod's law, $\mathrm{d}\Sigma/\mathrm{d}\Omega = (\text{constant})\Psi/Q^4$, for particles with a sufficiently sharp step of the electron distribution at the surface. Ψ is the surface area of the particle. From the crossover regime between Q^{-1} and Q^{-4}, the radius of the cross section of the rod R, and again the mass per length M/L, can be determined [by using eq 2 in a plot of $\log(Q\mathrm{d}\Sigma/\mathrm{d}\Omega)$ vs Q^2 (cf. Figure 3a,b)].

From Porod's law and the invariant $C = \int_0^\infty \mathrm{d}Q\, Q^2[\mathrm{d}\Sigma(Q)/\mathrm{d}\Omega] = (\text{constant})V$, the specific surface area $\Psi_S = \Psi/V$ can be calculated, where V is the volume of the particle. The radius R of a cylinder homogeneously filled with electrons can be derived from the specific surface area: $\Psi_S = \Psi/V \approx 2/R$.

For the cinerean samples with molecular masses between $\bar{M} = 165\,000$ Dalton and 100 000 Da (determined by low-angle laser light scattering) in water, we found $M/L = 2400 \pm 300$ Da nm^{-1} and the diameter $D = 2R = 1.7 \pm 0.2$ nm. In the concentration range used between 6 and 50 mg/mL, a concentration dependence of the values for M/L and R due to correlation or multiple scattering could not be found. In the range investigated, the measured macroscopic scattering cross sections normalized to the concentration $c^{-1}(\mathrm{d}\Sigma/\mathrm{d}\Omega)$ coincide within the errors (10%) (cf. Figure 4). In heavy water for different samples the corresponding values are

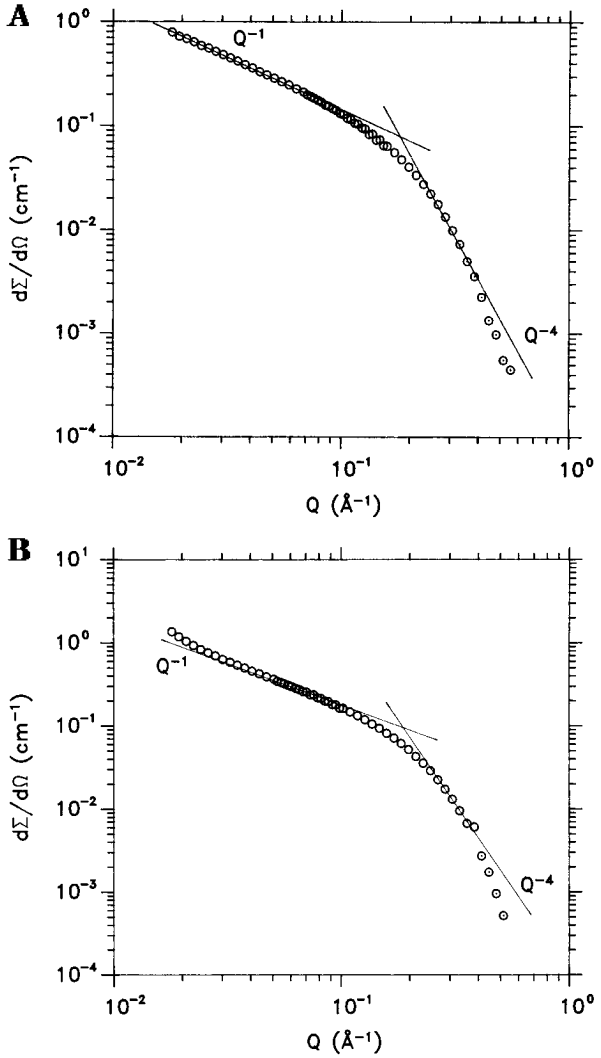

Figure 2. Typical scattering cross section for fragmented cinerean in H_2O (A) and in D_2O (B). The Q^{-1} and Q^{-4} regions can be recognized.

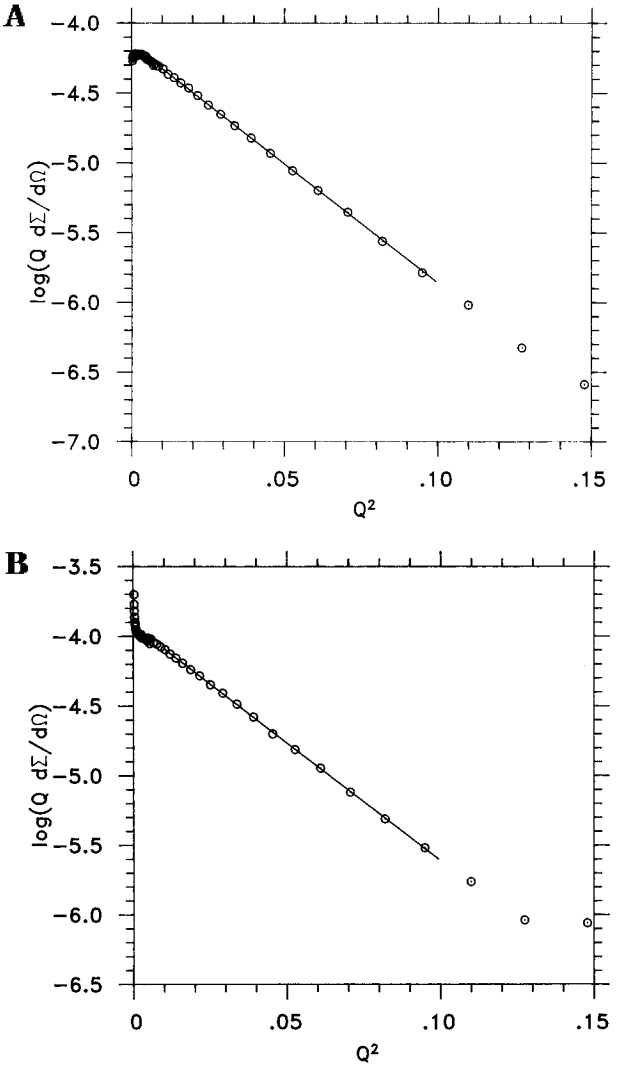

Figure 3. Plots to determine M/L and R from the crossover regime from Q^{-1} to Q^{-4}, using eq 2, (A) in H_2O and (B) in D_2O.

$M/L = 2120 \pm 370$ Da nm^{-1} and $D = 1.7 \pm 0.2$ nm. Within the errors, these are in agreement with the values for native cinerean ($M/L = 2250 \pm 490$ Da nm^{-1} and $D = 1.9 \pm 0.2$ nm) published in our previous paper.[9] From these results, a triple-helical conformation can also be concluded for the fragmented cinerean. It accounts for the rigidity of the rods. Calculated from the mass density by $D = 2R = \sqrt{2(M/L)/(\rho\pi)}$, the diameter of the rods, $D = 2R = 1.9 \pm 0.3$ nm, is in good agreement with the diameter obtained from the crossover regime. $\rho = 1.44$ g/cm^3 is the density of cinerean.[9]

X-ray Scattering in the Miscibility Gap. The result of an X-ray scattering experiment with one solution at two different temperatures is shown in Figure 5. The undercooled, turbid solution (in the coexistence regime) was studied (Figure 5) first at $T \approx 10$ °C. Then it was warmed in situ to above the clearing point ($T \approx 30$ °C; now monophasic) and measured again (Figure 5). (The data are without background subtraction; the peak on the right is caused by the polycarbonate windows of the sample holder.) The sample concentration was $c = 200$ mg/mL. This corresponds to a volume fraction $v_2 = 0.1217$ of the polymer. Concentration and volume fraction are connected by $v_2 = c/(c + \rho)$. The cloud point was at about 15 °C and the clearing point at 27 °C. They are marked in Figure 1.

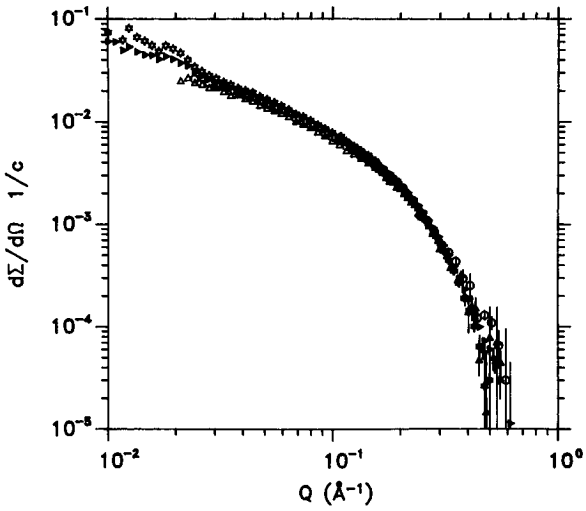

Figure 4. Scattering cross section of four solutions with concentrations between 6 and 50 mg/mL (normalized to the concentration). All points fall within the size of the circles and the errors; consequently, no concentration dependence of the values for M/L and R due to correlation or multiple scattering appears.

The background beneath the peak (0.28 Å^{-1} < Q < 0.48 Å) in the biphasic solution was interpolated with

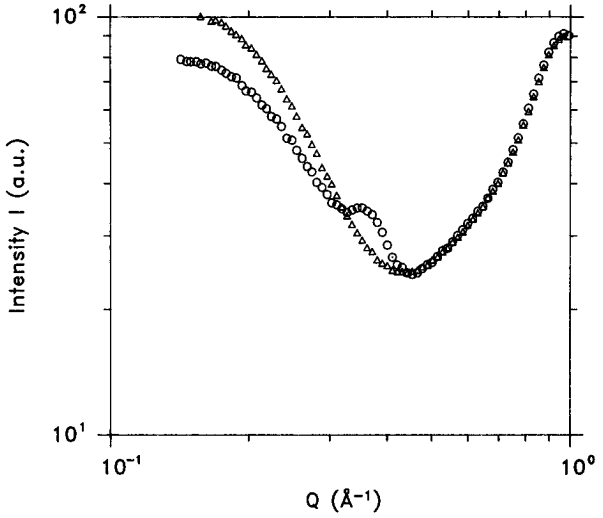

Figure 5. Angular average of the intensity on the two-dimensional detector: ○, solution in the miscibility gap; △, same solution, but in the isotropic phase at higher temperatures.

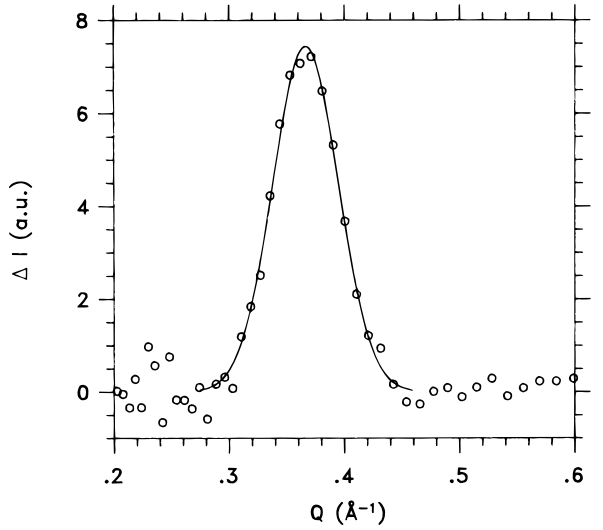

Figure 6. Gaussian fitted to the difference between measured and interpolated data.

a polynomial of sixth order. From the measured data, a data set calculated with the polynomial was subtracted. The result of this "background" subtraction is shown in Figure 6 together with a Gaussian fitted to the data points.

This peak can be interpreted as the angular average of a Debye−Scherrer ring.[18] If the rod axes in the domains are aligned in a regular, for example, hexagonal, pattern, diffraction maxima are expected according to Bragg's law, $m\lambda = 2d \sin\theta$, where m is the order of the diffraction maximum and d is the lattice constant (distance between the layers of the rods). Thus, the absolute values of the reciprocal lattice vectors are given by $2\pi m/d$. The domains are distributed randomly in the solution.

The location of the peak is $Q_M = 0.37$ Å^{-1}. By assuming close packing of the rods, this leads to a diameter of $D = 1.96 \pm 0.03$ nm. This value is consistent with the diameter of the rods in isotropic solutions. The alignment, and thus the order of the rods, is quite high. Peaks of higher order than $m = 1$ cannot be seen, because their intensity diminishes strongly with the structure factor of the rod.

Table 1. Results of X-ray Scattering in the Miscibility Gap

sample	solvent	Q_M (Å^{-1})	lattice constan d (nm)	thickness Λ (nm)
FC04	H_2O	0.367 ± 0.002	1.98 ± 0.03	34 ± 5
FC31-5-95	H_2O	0.373 ± 0.002	1.94 ± 0.03	44 ± 5

The peak width is very large compared to the excellent resolution of the small-angle instrument. Therefore, a resolution correction of the peak width is not necessary. From the peak width the dimensions of the precipitates (thickness) $\Lambda = Nd$ can be estimated with[18] $\Lambda = 0.9\lambda[\cos\theta_M\, \Delta'(2\theta)]$. Here λ is the wavelength and $\Delta'(2\theta)$ the angular width at half-maximum. The results are summarized in Table 1. The average value for the thickness of the precipitates is about 40 ± 5 nm. Correspondingly, one domain contains about 20 layers of rods.

In the turbid solution there is, in addition to the peak, still small-angle scattering from the isotropic phase (cf. Figure 5). By comparing the scattering of the clear and turbid solutions, it becomes obvious that intensity shifts from the small-angle part into the peak. This verifies that a biphasic solution exists where bundle-shaped domains of parallel and aligned rods are distributed randomly in an otherwise isotropic solution. We assume that the length of the bundles (domains) is as long as or longer than one rod. There is no indication of gelation; the solution remains liquid. The domains have a rather high degree of packing order and alignment.

Conclusions

In H_2O and D_2O solutions, fragmented cinerean has a rodlike, triple-helical conformation. It shows the phase separation of a liquid crystal and an isotropic phase that can be qualitatively explained by Flory's theory for rigid rods. In the biphasic solution the rods are aligned in parallel, forming bundle-shaped domains in an otherwise isotropic solution. This was shown by finding a Debye−Scherrer ring with X-ray scattering. The alignment of the rods is surprisingly perfect; the derived layer distance is consistent with the diameter determined by SAXS in the isotropic phase. The structure of the liquid-crystalline domains supports the predictions of Flory.

Acknowledgment. We thank U. Engelbrecht, G. Goerigk, H.-G. Haubold, P. Hiller, H. Jungbluth, A. Koschel, N. Monschau, M. Pionke, G. Schmidt, H. Sahm, and D. Schneiders for technical support and helpful discussions.

References and Notes

(1) Montant, C.; Thomas, L. *Ann. Sci. Nat. Bot. Veg.* **1977**, *18*, 185.
(2) Stahmann, K.-P.; Pielken, P.; Schimz, K. L.; Sahm, H. *Appl. Environ. Microbiol.* **1992**, *58*, 3347.
(3) Stone, B. A.; Clarke A. E. *Chemistry and biology of (1−3)-[beta]-glucans*; La Trobe University Press: Australia, 1992.
(4) Tabata, K. *Carbohydr. Res.* **1981**, *89*, 121.
(5) Franz, G., Ed. *Polysaccharide*; Springer: Berlin, Heidelberg, New York, 1991.
(6) Sutherland, I. W. Extracellular Polysaccharides. In *Biotechnology*; Rehm, H. J., Ed.; Springer: Heidelberg, 1983.
(7) Holzwarth, G. *Dev. Ind. Microbiol.* **1985**, *26*, 271.
(8) Ballauff, M. *Angew. Chem.* **1989**, *3*, 261.
(9) Stahmann, K.-P.; Monschau, N.; Sahm, H.; Koschel, A.; Gawronski, M.; Kopp, F.; Conrad, H.; Springer, T. *Carbohydr. Res.* **1995**, *266*, 115.

(10) Flory, P. J. *Proc. R. Soc. London A* **1956**, *234*, 73. Murthy, A. K.; Muthukumar, M. *Macromolecules* **1987**, *20*, 564. Miller, W. G.; Wu, C. C.; Wee, E. L.; Santee, G. L; Rai, J. H.; Goebel, K. G. *Pure Appl. Chem*. **1974**, *38*, 37.
(11) Kitamura, S.; Kuge, T. *Biopolymers* **1989**, *28*, 639.
(12) Norisuye, T.; Yanaki, T.; Fujita, H. *J. Polym. Sci., Polym. Phys. Ed*. **1980**, *18*, 547.
(13) Gawronski, M.; Aguirre, G.; Conrad, H.; Springer, T.; Stahmann, K.-P. Manuscript in preparation.
(14) Van, K.; Norisuye, T.; Teramoto, A. *Mol. Chyst. Liq. Chryst*. **1981**, *78*, 123. Van, K.; Teramoto, A. *Polym. J. (Tokyo)* **1982**, *14*, 999. Van, K.; Asakawa, T.; Teramoto, A. *Polym. J. (Tokyo)* **1984**, *16*, 65.
(15) Itou, T.; Teramoto, A.; Matsuo, T.; Suga, H. *Macromolecules* **1986**, *19*, 1234.
(16) Haubold, H. G.; Grünhagen, K.; Wagener, M.; Jungbluth, H.; Heer, H.; Pfeil, A.; Rongen, H.; Brandenberg, G.; Möller, R.; Matzerath, J.; Hiller, P.; Halling, H. *Rev. Sci. Instrum*. **1989**, *60*, 1943.
(17) Glatter, O.; Kratky, O. *Small Angle X-Ray Scattering*; Academic: New York, 1982.
(18) Guinier, A. *X-Ray Diffraction*; Freeman: San Francisco, London, 1963.

MA951368X